Local Structure Analysis by Isotropic Hilbert Transforms

Lennart Wietzke[1], Oliver Fleischmann[2], Anne Sedlazeck[2], and Gerald Sommer[2]

[1] Raytrix GmbH, Germany
[2] Cognitive Systems Group, Department of Computer Science, Kiel University

Abstract. This work presents the isotropic and orthogonal decomposition of 2D signals into local geometrical and structural components. We will present the solution for 2D image signals in four steps: signal modeling in scale space, signal extension by higher order generalized Hilbert transforms, signal representation in classical matrix form, followed by the most important step, in which the matrix-valued signal will be mapped to a so called multivector. We will show that this novel multivector-valued signal representation is an interesting space for complete geometrical and structural signal analysis. In practical computer vision applications lines, edges, corners, and junctions as well as local texture patterns can be analyzed in one unified algebraic framework. Our novel approach will be applied to parameter-free multilayer decomposition.

1 Introduction

Low level image analysis is often the first step of many computer vision tasks. Therefore, local signal features determine the quality of subsequent higher level processing steps. In this work we present a general 2D image analysis theory which is accurate and less time consuming (seven 2D convolutions are required), either because of its rotationally invariance. The first step of low level signal analysis is the designation of a reasonable signal model. Based on the fact that signals $f \in L^2(\Omega) \cap L^1(\Omega)$ with $\Omega \subseteq \mathbb{R}^2$ can be decomposed into their corresponding Fourier series, we assume that each frequency component of the original image signal consists locally of a superposition of intrinsically 1D (i1D) signals $f_\nu(z)$ with $z = (x, y) \in \mathbb{R}^2$, and $\nu \in \{1, 2\}$, see Equation (3). Each of them is determined by its individual amplitude $a_\nu \in \mathbb{R}$, phase $\phi_\nu \in [0, \pi)$ [1,2], and orientation $\theta_\nu \in [0, \pi)$. To access each one of those frequency components, an appropriate filter must be applied to the original signal. Although any scale space concept can be used, in this work we will choose the Poisson low pass filter kernel [3] $p(z; s)$ instead of the Gaussian kernel. The Poisson scale space is naturally related to the generalized Hilbert transform by the Cauchy kernel [4]. In Fourier space $\mathcal{F}\{\cdot\}$ [5] it can be seen that the well known derivative operator of order m

$$\mathcal{F}\{\mathcal{D}^{(m)}\}(u) = [2\pi\ u\ \mathbf{i}]^m \quad \text{with} \quad u \in \mathbb{R}^2 \tag{1}$$

is closely related to the generalized Hilbert transform operator of m concatenations

$$\mathcal{F}\{\mathcal{H}^{(m)}\}(u) = [2\pi\ \bar{u}\ \mathbf{i}]^m \quad \text{with} \quad \bar{u} = \frac{u}{\|u\|}\ . \tag{2}$$

M. Goesele et al. (Eds.): DAGM 2010, LNCS 6376, pp. 131–140, 2010.

2 Local Texture Modeling in Scale Space

Applying the Poisson filter kernel p to the original signal $\mathcal{P}_s\{f\}(z) = (p_s * f)(z)$ results in the smoothed signal model

$$f_p = \sum_{\nu=1}^{n} \underbrace{a_\nu \cos(\langle z, \bar{o}_\nu \rangle + \phi_\nu)}_{f_\nu(z)} \; \forall z \in \Omega \tag{3}$$

with $\bar{o}_\nu = [\cos\theta_\nu, \sin\theta_\nu]^T$ as the oriented normal, $\langle \cdot, \cdot \rangle$ as the inner product, and $*$ as the convolution operator. This local signal model allows modeling textures and structures such as lines, edges, corners, and junctions in scale space. After having specified the signal model, the mathematical task is the exact retrieval of the signal parameters $(\theta_\nu, \phi_\nu, a_\nu)$ for every position $z \in \Omega$, and for every scale space parameter $s > 0$. In the following f^e will be called the even signal part. Furthermore and without loss of generality, at the origin $(\mathbf{0}; s)$ with $\mathbf{0} = (0, 0)$ of the applied local coordinate system, the assumed signal model (3) results in

$$f_p = \mathcal{P}_s\{f\}(\mathbf{0}) = (p_s * f)(\mathbf{0}) = \sum_{\nu=1}^{n} \underbrace{a_\nu \cos\phi_\nu}_{f^e_\nu} \; . \tag{4}$$

Since the geometrical information θ_ν is not coded in the signal value f_p, an appropriate signal extension is necessary. Normally, this will be done by calculating higher order derivatives of the signal, e.g. the SIFT features [6]. This work generalizes and improves [7] by using higher order Hilbert transforms, and we will compare the results with those of using derivatives.

$$T = \left(\begin{bmatrix} \\ \\ \end{bmatrix} + \begin{bmatrix} \\ \\ \end{bmatrix} \mathbf{i} + \begin{bmatrix} \\ \\ \end{bmatrix} \mathbf{j} \right) * f$$

Fig. 1. Illustration of the convolution kernels in the spatial domain of the quaternion-valued matrix signal representation T

3 Signal Extension by Hilbert Transforms

The problem, which has to be solved now, is the search for all unknown structural parameters $a_\nu \in \mathbb{R}$ and $\phi_\nu \in [0, \pi)$ and the unknown geometric parameters $\theta_\nu \in [0, \pi)$. We will restrict the signal model (3) to $n < 3$, since by this restriction most signal structures can be modeled [8]. As the signal parameters are unknown, we have to solve an inverse problem. This can only be done by extending the original signal to result in a system of equations, which includes all unknown signal parameters. This will be done by the generalized Hilbert transforms of higher orders. Our signal model which consists of two superimposed i1D signals results in six degrees of freedom, which require generalized Hilbert transforms of up to order three. The first order Hilbert transform kernels read

$$\begin{bmatrix} h_x \\ h_y \end{bmatrix}(z) = \frac{1}{2\pi\|z\|^3} \begin{bmatrix} x \\ y \end{bmatrix} \tag{5}$$

which are the analogues to the first order partial derivatives. Since we have to analyze the original signal in scale space, it will be of advantage to provide one unified convolution kernel, which consists of the Poisson kernel and the generalized Hilbert transform kernel of order n. The generalized Hilbert transform of order $(i+j)$ in Poisson scale space reads

$$q_{x^i y^j}(z) = (\underbrace{h_x * \ldots * h_x}_{i} * \underbrace{h_y * \ldots * h_y}_{j} * p_s)(z) \; . \tag{6}$$

The value of the $(i+j)$th order Hilbert transformed signal in Poisson scale space will be derived by convolution in the spatial domain $f_{x^i y^j} = (q_{x^i y^j} * f)(z)$.

3.1 Signal Intelligence in Radon Space

After extending the original signal, the generalized Hilbert transformed signal must be interpreted. This can be done in Radon space by the relation to the Fourier slice theorem. The original signal f transformed into Radon space $f_r = \mathcal{R}\{f\}$ reads

$$f_r(t,\theta;s) = \int\limits_{z\in\mathbb{R}^2} \mathcal{P}_s\{f\}(z)\delta\left(\langle z,\bar{o}\rangle - t\right)\, dz \tag{7}$$

with $\theta \in [0,\pi)$ as the orientation, $t \in \mathbb{R}$ as the minimal distance of the parameterized line to the origin of the local coordinate system of the test point, and δ as the Dirac distribution. The corresponding inverse Radon transform $\mathcal{R}^{-1}$ exists. The $(i+j)$th order generalized Hilbert transformed signal can be expressed in Radon space, which delivers a system of equations of all unknown signal parameters. This system of equations can be solved, which has been done up to now only for $n = 1$ in Equation (3) [8]. The Hilbert transformed signal can be expressed by

$$f_{x^i y^j} = \mathcal{R}^{-1}\left\{\cos^i\theta \sin^j\theta \; h^{(i+j)}(t) * f_r(t;\theta;s)\right\}(z) \tag{8}$$

(Proof: Fourier slice theorem) with the classical one dimensional Hilbert transform kernel [9] of order m

$$h^{(m)}(t) = \begin{cases} \delta(t), & m \bmod 4 = 0 \\ \frac{1}{\pi t}, & m \bmod 4 = 1 \\ -\delta(t), & m \bmod 4 = 2 \\ -\frac{1}{\pi t}, & m \bmod 4 = 3 \end{cases}, t \in \mathbb{R} \tag{9}$$

with δ as the Dirac distribution, which is the algebraic neutral element of the convolution. Finally, the $(i+j)$th Hilbert transformed signal results in

$$f_{x^i y^j} = \sum_{\nu=1}^{n} \left[\cos^i\theta_\nu \sin^j\theta_\nu\right] f_\nu^{(i+j)} \tag{10}$$

(Proof: Linearity of the inverse Radon transform). The odd signal part $f_\nu^o = (h^{(1)} * f_\nu^e)(\phi_\nu) = a_\nu \sin\phi_\nu$ results of the even part by the classical 1D Hilbert transform and

$$f_\nu^{(m)} = \begin{cases} f_\nu^e, & m \bmod 4 = 0 \\ f_\nu^o, & m \bmod 4 = 1 \\ -f_\nu^e, & m \bmod 4 = 2 \\ -f_\nu^o, & m \bmod 4 = 3 \end{cases} \tag{11}$$

In case of the zeroth order Hilbert transform (i.e. $i + j = 0$), this results in the local signal value f_p. According to (10), the first and second order Hilbert transformed signal determines the following system of linear equations

$$\begin{bmatrix} f_x \\ f_y \end{bmatrix} = \sum_{\nu=1}^{n} \begin{bmatrix} \cos\theta_\nu \\ \sin\theta_\nu \end{bmatrix} f_\nu^o \tag{12}$$

and

$$\begin{bmatrix} f_{xx} \\ f_{xy} \\ f_{yy} \end{bmatrix} = \sum_{\nu=1}^{n} \begin{bmatrix} \cos^2\theta_\nu \\ \cos\theta_\nu \sin\theta_\nu \\ \sin^2\theta_\nu \end{bmatrix} f_\nu^e \tag{13}$$

from which the signal value can be reconstructed by $f_p = f_{xx} + f_{yy}$. With (10), the third order Hilbert transformed signal determines the following system of linear equations

$$\begin{bmatrix} f_{xxx} \\ f_{xxy} \\ f_{xyy} \\ f_{yyy} \end{bmatrix} = \sum_{\nu=1}^{n} \begin{bmatrix} \cos^3\theta_\nu \\ \cos^2\theta_\nu \sin\theta_\nu \\ \cos\theta_\nu \sin^2\theta_\nu \\ \sin^3\theta_\nu \end{bmatrix} f_\nu^o \tag{14}$$

from which the first order generalized Hilbert transform can be reconstructed by $f_x = f_{xxx} + f_{xyy}$ and $f_y = f_{xxy} + f_{yyy}$. Due to the relation of the Radon transform to the generalized Hilbert transform of any order, it is possible to result in a system of equations which can be now solved for the unknown signal parameters. Please note that neither the Radon transform nor its inverse are ever applied to the signal in practise. This is a very important advantage compared to the wavelet transforms (e.g. Ridgelet transforms [10]). Those approaches try out only a finite number of directions by the discrete Radon transform [10], which suffers from numerical problems. The resulting disadvantages are inaccuracy, problems resulting from aliasing effects, and higher computational time complexities.

4 Algebraic Signal Representation

Derivative based signal extensions are normally arranged in matrix or tensor form. Since these forms are only hardly suitable for geometric interpretation, we now present a signal representation in the so called multivector form, which comes from the field of geometric algebra [11]. Recent results of the hybrid matrix geometric algebra [12] offer geometric interpretation, which in our case enables the complete signal analysis by mapping tensor structures to multivectors. For the sake of simplicity, we will restrict this paper to the algebra of quaternions, which are solely needed for constructing the signal tensor. Loosely spoken, simply consider the tensor-valued signal extension as a real-valued $2 \times 2 \times 3$ array. According to [12], a mapping from the quaternion-valued tensor

$T \in M(2,\mathbb{H})$ to the quaternion-valued vector $\varphi(T) \in \mathbb{H}^3$ is possible. With the set of basis vectors $\{1, \mathbf{i}, \mathbf{j}, \mathbf{k}\}$ of the quaternions $\mathbb{H}$, the signal tensor for $n < 3$ in Equation (3) can be defined by the generalized Hilbert transforms of second and third order

$$T = \begin{bmatrix} f_{xx} & f_{xy} \\ f_{xy} & f_{yy} \end{bmatrix} + \begin{bmatrix} f_{xxx} & f_{xxy} \\ f_{xxy} & f_{xyy} \end{bmatrix} \mathbf{i} + \begin{bmatrix} f_{xxy} & f_{xyy} \\ f_{xyy} & f_{yyy} \end{bmatrix} \mathbf{j} \,,$$

see Figure 1. By introducing the abbreviations $f^- = f_{xx} - f_{yy}$, $f_x^- = f_{xxx} - f_{xyy}$ and $f_y^- = f_{xxy} - f_{yyy}$ the quaternion-valued matrix T can be mapped by the isomorphism φ to a quaternion-valued vector representation

$$\varphi(T) = \begin{bmatrix} \frac{f_p}{2} \\ f_{xy} \\ \frac{f^-}{2} \end{bmatrix} + \begin{bmatrix} \frac{f_x}{2} \\ f_{xxy} \\ \frac{f_x^-}{2} \end{bmatrix} \mathbf{i} + \begin{bmatrix} \frac{f_y}{2} \\ f_{xyy} \\ \frac{f_y^-}{2} \end{bmatrix} \mathbf{j} \tag{15}$$

which will be called signal multivector, see Figure (2). The signal multivector delivers the complete geometrical and structural signal information with respect to both the assumed signal model and the assumed maximal order of Hilbert transforms. In [13] the geometrical signal features have been retrieved by higher order derivatives in the traditional matrix expression. This will be generalized by $\varphi(T)$ in a more natural embedding.

$$\varphi(T) = \left(\begin{bmatrix} \\ \\ \\ \end{bmatrix} + \begin{bmatrix} \\ \\ \\ \end{bmatrix} \mathbf{i} + \begin{bmatrix} \\ \\ \\ \end{bmatrix} \mathbf{j} \right) * f$$

Fig. 2. Illustration of the convolution kernels in the spatial domain of the signal multivector $\varphi(T)$ which is defined in Equation (15)

4.1 Geometry from the Signal Multivector

The hardest challenge of our signal analysis problem is to obtain the exact geometrical signal features such as the orientations θ_ν. The most important relations are

$$\sin(2\theta_{2/1}) = \frac{1}{\det D_{1/2}} \det \begin{bmatrix} f_{xxy} & \cos\theta_{1/2} \\ f_{xyy} & \sin\theta_{1/2} \end{bmatrix} \tag{16}$$

and

$$\cos(2\theta_{2/1}) = \frac{1}{\det D_{1/2}} \det \begin{bmatrix} \frac{f_x^-}{2} & \cos\theta_{1/2} \\ \frac{f_y^-}{2} & \sin\theta_{1/2} \end{bmatrix} \tag{17}$$

with the matrix

$$D_{1/2} = \begin{bmatrix} \frac{f_x}{2} & \cos\theta_{1/2} \\ \frac{f_y}{2} & \sin\theta_{1/2} \end{bmatrix} \tag{18}$$

which follow from Equation (14) of the third order generalized Hilbert transform for $n = 2$. From the fact that $\sin^2(2\theta_{2/1}) + \cos^2(2\theta_{2/1}) = 1$, the nonlinear part of the

inverse problem follows in form of a quadratic equation (since two unknown orientations have to hold the equation)

$$\gamma^- \sin^2 \theta_\nu + \alpha \sin(2\theta_\nu) = \beta \tag{19}$$

with

$$\delta = \left[\frac{f_x}{2}\right]^2 - f_{xxy}^2 - \left[\frac{f_x^-}{2}\right]^2 \tag{20}$$

$$\beta = \left[\frac{f_y}{2}\right]^2 - f_{xyy}^2 - \left[\frac{f_y^-}{2}\right]^2 \tag{21}$$

$$\alpha = \frac{f_x}{2}\frac{f_y}{2} - f_{xxy} f_{xyy} - \frac{f_x^-}{2}\frac{f_y^-}{2} \tag{22}$$

$$\gamma^+ = \beta + \delta \tag{23}$$

$$\gamma^- = \beta - \delta \tag{24}$$

The main orientation can be derived by

$$\theta_1 + \theta_2 = \arctan \frac{2\alpha}{\gamma^-} \tag{25}$$

as well as the apex angle

$$\|\theta_1 - \theta_2\| = \arctan \frac{2\sqrt{\alpha^2 - \beta\delta}}{\gamma^+} \tag{26}$$

from which the single orientations θ_ν can be obtained separately. Note, that geometric algebra offers a more natural embedding of the signal multivector and delivers these results by a single operation, called the geometric product.

4.2 Structure from the Signal Multivector

The local phase and amplitude represent the structural signal features, which can be calculated by solving a linear system of equations by the Cramer's rule of 2×2 matrices. The even and odd signal parts can be derived by

$$\begin{bmatrix} f_1^e \\ f_2^e \end{bmatrix} = \frac{1}{\sin(\theta_1 - \theta_2)\cos(\theta_1 + \theta_2)} \begin{bmatrix} \frac{f_p}{2}\sin(2\theta_2) - f_{xy} \\ f_{xy} - \frac{f_p}{2}\sin(2\theta_1) \end{bmatrix} \tag{27}$$

which has been derived by the second order generalized Hilbert transform and

$$\begin{bmatrix} f_1^o \\ f_2^o \end{bmatrix} = \frac{1}{\sin(\theta_1 - \theta_2)} \begin{bmatrix} f_y \cos\theta_2 - f_x \sin\theta_2 \\ f_x \sin\theta_1 - f_y \cos\theta_1 \end{bmatrix} \tag{28}$$

which has been derived by the first order generalized Hilbert transform respectively. By means of the even and odd signal parts, finally the structural signal features such as the phases and the amplitudes can be derived by

$$\phi_\nu = \arctan \frac{f_\nu^o}{f_\nu^e} \tag{29}$$

$$a_\nu = \sqrt{[f_\nu^e]^2 + [f_\nu^o]^2} \tag{30}$$

for $\nu \in \{1, 2\}$. Interestingly, this solution corresponds for each signal component to the classical 1D analytic signal [14].

5 Applications and Experimental Results

The signal multivector is isotropic and therefore needs only seven convolution filters. The signal multivector can be implemented either in Fourier space or in the spatial domain. But the advantage of the spatial domain is the local adaption on the individual scale space parameter which carries the important signal information for each test point. Because of that we favor the convolution in the spatial domain. The implementation of the signal multivector is easy and can be calculated in $O(m)$ with m as the total convolution mask size. In practice the convolution mask size involves 7×7 pixels. Due to the latest developments in graphic controllers, the signal multivector can be also implemented directly using the OpenGL® Shading Language (GLSL). This enables realtime computation of the signal multivector and detecting its optimal scale space parameter by maximizing the local amplitude for each test point individually [8]. Since the signal multivector is a fundamental low-level approach, many applications can be found. In the following we will present the parameter-free decomposition of multilayer textures.

5.1 Multilayer Decomposition

As an application of the signal multivector we will analyze superimposed oriented patterns and compare our results with the derivative based approach presented in [15]. In comparison to [15] our approach does not need any parameter tuning and unifies the case of i1D and i2D signals in one framework.

Derivative based approach. In [15] an i1D signal is assumed at first. An evidence check decides between computation of one single orientation or the double orientation case. The derivative operator for one orientation θ reads

$$\mathcal{D}_\theta = \cos\theta \frac{\partial}{\partial x} + \sin\theta \frac{\partial}{\partial y} \tag{31}$$

In the i1D case, the orientation computation is in essence an eigenspace analysis of the tensor $T = \nabla f \nabla f^T$ computed over a neighborhood Ω. The confidence measure for an i1D structure is determined as $\det(T) \leq \lambda \ \mathrm{trace}^2(T)$ with the tuning parameter $\lambda > 0$ which has to be chosen manually. In the i2D case, the comparison in this paper is restricted to considering overlaid oriented patterns resulting in the model

$$f(z) = \sum_{\nu=1}^{2} f_\nu(z) \quad \text{with } z = (x, y) \in \Omega \tag{32}$$

Using the derivative operator (31) and applying it to the double orientation case, the image signal in Gaussian scale space $\mathcal{G}\{\cdot\}(z; s)$ satisfies the equation

$$\mathcal{D}_{\theta_1} \mathcal{D}_{\theta_2} \mathcal{G}\{f\}(z; s) = c^T \mathcal{D} f = 0 \tag{33}$$

with the so called mixed-orientation vector

$$c = [\cos\theta_1 \cos\theta_2, \sin(\theta_1 + \theta_2), \sin\theta_1 \sin\theta_2]^T \tag{34}$$

and

$$\mathcal{D} f = \left[\frac{\partial^2}{\partial x^2}, \frac{\partial^2}{\partial x y}, \frac{\partial^2}{\partial y^2} \right]^T \mathcal{G}\{f\}(z; s) \tag{35}$$

Taking into account that real image signals do not satisfy Equation (33) exactly the residual error is defined by

$$\varepsilon(c) = c^T \underbrace{\left[\int_{z \in \Omega} (\mathcal{D}f)(\mathcal{D}f)^T \, dz \right]}_{J} c \tag{36}$$

which has to be minimized with respect to the vector c under the constraint $c^T c = 1$. The eigenvector analysis of the 3×3 tensor J allows the computation of the mixed-orientation vector c up to an unknown scaling factor $r \in \mathbb{R}$ by using the minors of J. In a second test based on the properties of J, the i2D case is confirmed, otherwise, the i0D case is assumed. In the i2D case, the vector rc has to be solved for the unknown orientations θ_1 and θ_2.

Comparison: signal multivector versus derivatives. Both methods have been tested on a set of synthetic and real images. The experiments on synthetic data have been conducted on patchlets with same size as the convolution kernels. Two overlaid structures have been tested in all possible combinations of angles, see Table (1). In addition, the performance of both methods in case of changing convolution kernel size and changing phase has been determined, see Figure (3). In case of the method [15] applied to real

Table 1. Signal multivector (SMV) average angular error (AAE) of the apex angle θ_a and the main orientation θ_m of junctions and multilayer signals

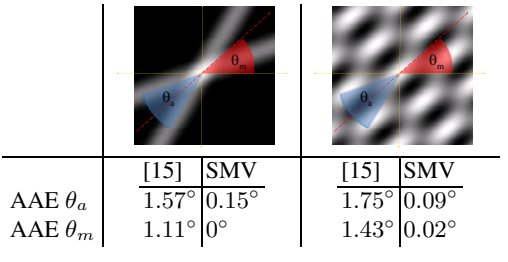

	[15]	SMV	[15]	SMV
AAE θ_a	1.57°	0.15°	1.75°	0.09°
AAE θ_m	1.11°	0°	1.43°	0.02°

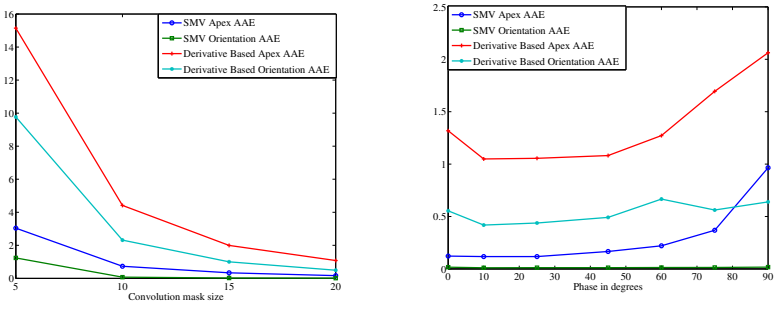

Fig. 3. Left figure: Average angular error (AAE) of [15] and the signal multivector (SMV) against varying convolution mask size. The signal multivector performs better with small size which is very important for local feature detection. Right figure: Average angular error (AAE) of [15] and the signal multivector (SMV) against varying signal phase.

images, it was sometimes difficult to adjust the parameter λ deciding between i1D and i2D signals, whereas the signal multivector based method only needs the scale space parameters, which can be adjusted automatically by phase congruency.

6 Conclusion

We have solved a fundamental problem of isotropic signal analysis with applications in parameter-free multilayer decomposition. Our novel approach can be described for arbitrary signal models by the following general steps

1. Signal modeling in scale space and signal extension by the generalized Hilbert transform. The order of the required generalized Hilbert transforms corresponds to the complexity n of the signal model in Equation (3).
2. Retrieving the explicit system of equations including all unknown signal parameters $(\theta_\nu, \phi_\nu, a_\nu)$ by the relation of the generalized Hilbert transform to the Radon transform.
3. Algebraic signal representation in tensor form and subsequent mapping by the isomorphism φ to its corresponding signal multivector.
4. Geometric interpretation of the signal multivector by solving the nonlinear part of the inverse problem.
5. Structural multivector-valued signal interpretation by solving the linear part of the inverse problem.

The message of this contribution is that the signal multivector is isotropic for i1D and two superimposed i1D signals and offers accuracy with less computational time. Future work contains the generalization of the signal multivector to multidimensional signal domains to enable also isotropic motion tracking in computer vision applications.

References

1. Oppenheim, A.V., Lim, J.S.: The importance of phase in signals. Proceedings of the IEEE 69(5), 529–541 (1981)
2. Huang, T., Burnett, J., Deczky, A.: The importance of phase in image processing filters. IEEE Trans. on Acoustics, Speech and Signal Processing 23(6), 529–542 (1975)
3. Felsberg, M., Sommer, G.: The monogenic scale-space: A unifying approach to phase-based image processing in scale-space. Journal of Mathematical Imaging and Vision 21, 5–26 (2004)
4. Delanghe, R.: On some properties of the Hilbert transform in Euclidean space. Bull. Belg. Math. Soc. Simon Stevin 11(2), 163–180 (2004)
5. Köthe, U., Felsberg, M.: Riesz-transforms vs. derivatives: On the relationship between the boundary tensor and the energy tensor. In: Kimmel, R., Sochen, N.A., Weickert, J. (eds.) Scale-Space 2005. LNCS, vol. 3459, pp. 179–191. Springer, Heidelberg (2005)
6. Lowe, D.G.: Distinctive image features from scale-invariant keypoints. International Journal of Computer Vision 60, 91–110 (2004)
7. Wietzke, L., Sommer, G., Fleischmann, O.: The geometry of 2D image signals. In: IEEE Computer Society on Computer Vision and Pattern Recognition, CVPR 2009, pp. 1690–1697 (2009)
8. Felsberg, M.: Low-level image processing with the structure multivector. Technical Report 2016, Kiel University, Department of Computer Science (2002)

9. Hahn, S.L.: Hilbert Transforms in Signal Processing. Artech House Inc., Boston (1996)
10. Pan, W., Bui, T.D., Suen, C.Y.: Rotation invariant texture classification by ridgelet transform and frequency-orientation space decomposition. Signal Process. 88(1), 189–199 (2008)
11. Perwass, C.: Geometric Algebra with Applications in Engineering. Geometry and Computing, vol. 4. Springer, Heidelberg (2009)
12. Sobczyk, G., Erlebacher, G.: Hybrid matrix geometric algebra. In: Li, H., Olver, P.J., Sommer, G. (eds.) IWMM-GIAE 2004. LNCS, vol. 3519, pp. 191–206. Springer, Heidelberg (2005)
13. Danielsson, P.E., Lin, Q., Ye, Q.Z.: Efficient detection of second-degree variations in 2D and 3D images. Journal of Visual Communication and Image Representation 12(3), 255–305 (2001)
14. Gabor, D.: Theory of communication. Journal IEE, London 93(26), 429–457 (1946)
15. Stuke, I., Aach, T., Barth, E., Mota, C.: Analysing superimposed oriented patterns. In: 6th IEEE Southwest Symposium on Image Analysis and Interpretation, pp. 133–137. IEEE Computer Society, Los Alamitos (2004)